Microporous and Mesoporous Materials 330 (2022) 111563

Contents lists available at ScienceDirect

Microporous and Mesoporous Materials

journal homepage: www.elsevier.com/locate/micromeso

Multiple equilibria describe the complete adsorption isotherms of nonporous, microporous, and mesoporous adsorbents

Gion Calzaferri [a,*], Samuel H. Gallagher [b], Dominik Brühwiler [b,**]

[a] Department of Chemistry, Biochemistry and Pharmaceutical Sciences, Freiestrasse 3, 3012 Bern, Switzerland
[b] Institute of Chemistry and Biotechnology, Zurich University of Applied Sciences (ZHAW), 8820 Wädenswil, Switzerland

ARTICLE INFO

Keywords:
Stöber-type particles
Zeolite L
MCM-41
Type I
Type II
Type IV
Type VI adsorption isotherms
Cluster
Cavity
Sequential chemical equilibria

ABSTRACT

The adsorption of simple gases begins with the formation of a monolayer on the pristine surface, not always followed by the formation of a second or more monolayers. Subsequently, cluster formation or cavity filling occurs, depending on the properties of the surface. The characteristically different shape of the isotherms related to these processes allows to clearly differentiate them. We analyzed argon and N_2 adsorption isotherms quantitatively over the entire relative pressure range for adsorbents bearing different properties: the nonporous Stöber-type particles, the microporous zeolite L (ZL) and zeolite L filled with indigo (Indigo-ZL), and three mesoporous silica adsorbents of different pore size. The formal equilibria involved in cluster formation and in cavity filling have been derived and successfully applied to quantitatively describe the isotherms of the adsorbents. No indication regarding formation of a second monolayer on top of the first one was observed for the Stöber-type particles. Instead, cluster generation, which minimizes surface tension, starts early. The behavior of microporous ZL and of Indigo-ZL is different. A second monolayer sets up and cluster formation starts with some delay. The enthalpy of cluster formation is, however, practically identical with that seen for the Stöber-type particles. The difference between the experimental and the calculated inflection points is very small. The shapes of the isotherms seen for the mesoporous adsorbents differ significantly from those seen for the nonporous and for the microporous adsorbents. The quantitative analysis of the data proves that formation of a second monolayer is followed by filling of cavities which ends as soon as all cavity sites are filled. The sum of the individual fractional contributions, namely the monolayer formation Θ_{mL}, the appearance of a second monolayer Θ_{2L} on top of the first one, and the cavity filling Θ_{cav}, yields a calculated adsorption isotherm Θ_{calc} which describes the experimental data Θ_{exp} well. The experimental and the calculated first inflection points are in excellent agreement, which is also the case for the second inflection points. The value of the cavity filling enthalpy is roughly 10% larger than that for the cluster formation seen in the nonporous and the microporous adsorbents. The volume for cavity filling is significantly smaller than the monolayer volume for the mesoporous adsorbent with a pore diameter of 2.7 nm, while it is the same or larger for pore diameters of 4.1 nm and 4.4 nm, respectively. We conclude that understanding the adsorption isotherms as signature of several sequential chemical equilibrium steps provides additional information data for clusters, cavities, and position of the inflection points, not accessible by means of the conventional models. The theory reported herein covers type I, II, IV and to some extent also type VI isotherms.

1. Introduction

An important goal when studying adsorption isotherms is to determine the specific surface area A_{mL}, the volume V_{mL} of adsorptive bound as a monolayer, and the binding strength measured by the enthalpy $\Delta_{ads}H^{\varnothing}$ of adsorption [1–9]. This information refers to the low relative pressure range of the isotherm to make sure that the data are characteristic of the adsorptive-adsorbent interaction. A successful theory that allows obtaining the desired knowledge goes back to Irving Langmuir who already in 1918 mentioned that a surface can consist of different

* Corresponding author.
** Corresponding author.
E-mail addresses: gion.calzaferri@unibe.ch (G. Calzaferri), dominik.bruehwiler@zhaw.ch (D. Brühwiler).
URL: https://calzaferri.dcbp.unibe.ch (G. Calzaferri), http://www.zhaw.ch/icbt/polymer (D. Brühwiler).

https://doi.org/10.1016/j.micromeso.2021.111563
Received 22 September 2021; Received in revised form 4 November 2021; Accepted 8 November 2021
Available online 15 November 2021

sites and that in such cases isotherms should be described as a linear combination of individual isotherms [10,11]. This led, many years later, to the description of systems consisting of several sites with different ease of adsorption and for multi-component gas analysis by means of DSL, dual-site Langmuir, and DPL, dual-process Langmuir [12–27]. We have extended the analysis of multiple equilibria of compounds with different coordination sites [28] to the explanation of adsorption isotherms for adsorbates bearing different sites, focusing on the low relative pressure range, i.e., on conditions where the adsorptive-adsorbent binding strength is larger than the adsorptive-adsorbate, so that monolayer coverage is favored [29]. We found on a rigorous basis that this leads to Langmuir's equation for each site independently, so that the total fractional amount of bound adsorptive can be described as linear combination of individual Langmuir isotherms. This allows to accurately determine the specific surface area, the volume of adsorptive bound as a monolayer, and the adsorption enthalpy. We are now interested in understanding the adsorption process taking place once monolayer coverage has been realized. The related problem can be well specified by observing the difference between the experimental adsorption isotherm and the monolayer coverage as a function of the relative pressure p_{rel} of the adsorptive. The relative pressure p_{rel} is defined by eqn (1), where p is the experimental pressure and p_0 is the saturation pressure of the gas at the experimental temperature.

$$p_{rel} = \frac{p}{p_0} \tag{1}$$

It is convenient to picture the isotherms by using the notion of the fractional coverage Θ, which is defined by the volume adsorbed V_{ads} at a given relative pressure p_{rel} divided by the complete monolayer adsorption volume V_{mL}, according to eqn (2). This allows a more comprehensible view of the properties of different adsorbents and of the different adsorption processes.

$$\Theta = \frac{V_{ads}}{V_{mL}} \tag{2}$$

The adsorption of simple gases begins with the formation of a monolayer on the pristine surface, not always followed by formation of second or supplementary layers. Subsequently, cluster formation or cavity filling occurs, depending on the properties of the surface. The characteristically different shape of the isotherms related to these processes allows clear differentiation. It is therefore interesting to study the difference ΔΘ between the experimental adsorption isotherm Θ_{exp} and the monolayer coverage Θ_{mL} as a function of the relative pressure p_{rel}. This is expressed by eqn (3).

$$\Delta\Theta = \Theta_{exp} - \Theta_{mL} \tag{3}$$

We use the Θ_{mL} data reported in Ref. [29]. The calculated difference ΔΘ is illustrated in Fig. 1 for three different adsorbents, nonporous Stöber-type silica particles [30], microporous zeolite L [31,32], and mesoporous silica, average pore diameter of 4.4 nm [33,34]. The isotherm (A) is classified according to IUPAC as type II, (B) as type I and (C) as type IV [5,6]. Further examples can be seen in Figs SI1-SI4. The blue curves represent the experimental values Θ_{exp}. The monolayer coverage isotherm Θ_{mL} is shown as red line. Its shape corresponds to type I isotherms. The difference ΔΘ is shown as black dash-dot line.

We observe that the difference ΔΘ between the experimental data and the monolayer coverage is of characteristically different shape for the three types of adsorbents. The ΔΘ curve for the nonporous Stöber-type particles seen in Fig. 1(A) shows a constant rise of the total volume of additional adsorptive bound with increasing pressure. This means that the adsorption isotherm Θ_{exp} consists of the first formed monolayer described by Θ_{mL} and of surface tension minimizing clusters formed on top of it at larger relative pressure. There is no upper limit for cluster formation. We express the corresponding fractional coverage by Θ_{clust}. The process results finally in condensation when approaching saturation pressure. We do not describe the condensation process but focus on the adsorption including cluster formation at the surface of the previously formed monolayer. We analyze data up to $p_{rel} \leq 0.9$ in order to avoid the region where condensation in inter-particle voids may start to contribute. The adsorption isotherm in terms of the fractional coverage Θ can therefore be expressed by means of eqn (4).

$$\Theta = \Theta_{mL} + \Theta_{clust} \tag{4}$$

The S-shape of the ΔΘ curve for the microporous zeolite L in Fig. 1(B) indicates the presence of two sequential processes. Zeolite L shows a 30% larger enthalpy of adsorption than seen for the Stöber-type particles (see Table 2, ref [29]). This indicates that the monolayer is more strongly bound to the polar surface of zeolite L. Therefore, extensive monolayer coverage is already realized at small relative pressure. The consequence is that the probability of building a second monolayer, the corresponding fractional coverage we express by Θ_{2L}, on top of the first one increases and cluster formation starts at a later stage, a fact that should be reflected by the binding strength. Eqn (4) must be extended as expressed in eqn (5) as a consequence. We further observe that the total volume of adsorptive bound by these two processes is much smaller than V_{mL}. This is understandable because the micropores are already filled and only the outer surface of the particles is accessible.

$$\Theta = \Theta_{mL} + \Theta_{2L} + \Theta_{clust} \tag{5}$$

A different situation is seen for the mesoporous silica adsorbent in Fig. 1(C). The ΔΘ curve shows, after an initial period, first a moderate increase followed by a step and a nearly flat continuation. This also indicates the formation of a second monolayer, despite the fact that the enthalpy of adsorption is identical to that of the Stöber-type particles (see Table 2, ref [29]). This is followed by the almost instantaneous filling of cavities that ends as soon as all cavity sites are completely filled

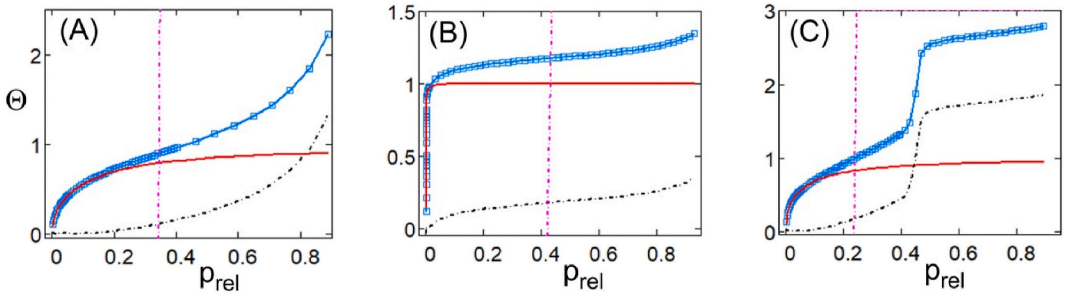

Fig. 1. Adsorption isotherms of Ar versus the relative pressure p_{rel}, measured at 87 K for a nonporous (A), a microporous (B), and a mesoporous (C) adsorbent. The blue lines with the squares are the experimental data Θ_{exp}. The red lines show the shape of the monolayer adsorption coverage Θ_{mL}. The black dash-dot lines are the difference ΔΘ between the experimental Θ_{exp} and the monolayer formation isotherms Θ_{mL}, eqn (3). The position of the experimental inflection point is shown as pink vertical dash-dot line. (A) Stöber-type particles; $V_{mL} = 3.7$ cm^3/g. (B) Zeolite L; $V_{mL} = 88$ cm^3/g (C) MCM-41 (4.4 nm); $V_{mL} = 251$ cm^3/g [29]. (For interpretation of the references to colour in this figure legend, the reader is referred to the Web version of this article.)

[35]. The volume of available cavities defines the upper limit of the process. This is in contrast to the cluster growth. We describe the cavity filling fractional coverage using Θ_{cav}. The experimental adsorption isotherm can therefore be expressed by means of eqn (6A) in absence and as eqn (6B) in presence of a second monolayer. The total volume of adsorptive bound by the cavity filling amounts to approximately twice the value of V_{mL} for monolayer coverage.

$$\Theta = \Theta_{mL} + \Theta_{cav} \tag{6A}$$

$$\Theta = \Theta_{mL} + \Theta_{2L} + \Theta_{cav} \tag{6B}$$

The goal of this study is to describe and to test this qualitative description quantitatively. This means that we attempt to understand the processes by means of equations that allow expressing fractional coverage for cluster formation Θ_{clust} and for cavity filling Θ_{cav} as a function of the relative pressure p_{rel}. There is a natural way to achieve this goal, namely by expressing the processes involved as multiple equilibria, as we have done for describing, e.g., cation exchange of zeolites [28] and for interpreting the adsorption isotherms of nonporous, microporous, and mesoporous adsorbents in the low relative pressure range [29]. We show that following this strategy leads to two expressions, one of them describing the cluster formation Θ_{clust} and the other the cavity filling Θ_{cav} as a function of the relative pressure p_{rel}. The basis for both is the same, but the consequences differ by the fact that the sudden filling of cavities ends as soon as all cavity sites are occupied, while cluster formation is not limited by this condition. The results are tested by applying them to a significant number of different adsorption isotherms mostly with Ar as adsorptive and some with N_2. Enthalpies of adsorption, inflection points, and the volume adsorbed by cluster formation or cavity filling are determined. Our results fill a longstanding gap as complete isotherms, not only a specific part, can be described based on the same principle, namely by analyzing multiple chemical equilibria, and that we can quantitatively distinguish between the different steps involved in the adsorption process.

2. Experimental

2.1. Materials

The Stöber-type silica particles were synthesized and characterized as reported in Ref. [29]. Zeolite L (ZL) and Indigo-Zeolite L (Indigo-ZL) are described in Refs. [29,36]. The synthesis of the MCM-41 type mesoporous silica materials with an average pore diameter of 4.4 nm, 4.1 nm and 2.7 nm is reported in Ref. [29].

2.2. Physical measurements

Prior to sorption measurements, the samples were vacuum-degassed at 150 °C for 3 h. The adsorption isotherms were measured with a Quantachrome Autosorb iQ MP. A CryoCooler was used for the measurement of argon adsorption at 87 K. Measurements at 77 K were conducted by cooling with a liquid nitrogen bath. The saturation vapor pressure p_0 was experimentally determined during the measurements.

2.3. Data analysis

The Levenberg-Marquardt method [37] was used for the numerical evaluation of the experimental data and to determine the parameters. It is important to first analyze the low relative pressure region, so that the monolayer coverage isotherm can be characterized separately. The higher relative pressure region can then be analyzed with high accuracy as reported in the theoretical section. Mathcad features for solving problems analytically and numerically were used to determine the inflection points [38].

3. Theory

The cluster formation and the cavity filling equilibria can be expressed as reported in Table 1. X denotes the concentration of adsorptive and L symbolizes the concentration of surface positions on which the clusters are formed or, respectively, the concentration of cavity positions where X can be adsorbed. Hence, both processes are represented by sequential equilibria, similar to what we have discussed in Ref. [28]. There is a formal resemblance to the equilibria formulated for protein interactions with small molecules [39].

It is convenient to express the equilibria in Table 1 by means of the stoichiometry matrix as explained in Refs. [41–43], where the labels with the bar are the logarithm of the corresponding object: $\overline{value} = \log(value)$. We further use $c_i = [LX_i]/c^{\varnothing}$ and hence: $\bar{c}_i = \log([LX_i]/c^{\varnothing})$. This allows writing eqn (7):

$$\begin{pmatrix} 1 & -1 & 0 & 0 & 0 & 0 & 0 & 0 & -1 \\ 0 & 1 & -1 & 0 & 0 & 0 & 0 & 0 & -1 \\ 0 & 0 & 1 & -1 & 0 & \cdot & \cdot & 0 & -1 \\ \cdot & \cdot & \cdot & \cdot & \cdot & \cdot & \cdot & \cdot & \\ \cdot & \cdot & \cdot & \cdot & \cdot & \cdot & \cdot & \cdot & \\ \cdot & \cdot & \cdot & \cdot & 0 & \cdot & -1 & 0 & -1 \\ 0 & 0 & 0 & 0 & \cdot & \cdot & 1 & -1 & -1 \end{pmatrix} \begin{pmatrix} \overline{c_n} \\ \overline{c_{n-1}} \\ \overline{c_{n-2}} \\ \cdot \\ \cdot \\ \cdot \\ \overline{c_0} \\ \overline{X} \end{pmatrix} = \begin{pmatrix} \overline{K}_n \\ \overline{K}_{n-1} \\ \overline{K}_{n-2} \\ \cdot \\ \cdot \\ \cdot \\ \overline{K}_1 \end{pmatrix} \tag{7}$$

Linear transformation of this equation leads to the solution we express in eqn (8) [42,43].

$$\begin{pmatrix} 1 & 0 & 0 & 0 & 0 & 0 & 0 & -1 & -n \\ 0 & 1 & 0 & 0 & 0 & 0 & 0 & -1 & -(n-1) \\ 0 & 0 & 1 & 0 & 0 & \cdot & \cdot & -1 & -(n-2) \\ \cdot & \cdot & \cdot & \cdot & \cdot & \cdot & \cdot & \cdot & \cdot \\ \cdot & \cdot & \cdot & \cdot & \cdot & \cdot & \cdot & \cdot & \cdot \\ \cdot & \cdot & \cdot & \cdot & \cdot & \cdot & 0 & -1 & -2 \\ 0 & 0 & 0 & 0 & \cdot & \cdot & 1 & -1 & -1 \end{pmatrix} \begin{pmatrix} \overline{c_n} \\ \overline{c_{n-1}} \\ \overline{c_{n-2}} \\ \cdot \\ \cdot \\ \cdot \\ \overline{c_0} \\ \overline{X} \end{pmatrix} = \begin{pmatrix} \overline{K}_n + \overline{K}_{n-1} + \ldots + \overline{K}_1 \\ \overline{K}_{n-1} + \overline{K}_{n-2} + \ldots + \overline{K}_1 \\ \overline{K}_{n-2} + \overline{K}_{n-3} + \ldots + \overline{K}_1 \\ \cdot \\ \cdot \\ \cdot \\ \overline{K}_1 \end{pmatrix} \tag{8}$$

It is natural within this context to choose $\overline{X}$ and $\overline{c_0}$ as free variables. This allows writing eqn (9).

$$\overline{c_i} = \overline{c_0} + i\overline{X} + \sum_{j=1}^{i} \overline{K_j} \tag{9}$$

The form of eqn (9) becomes now more useful:

Table 1
Sequential equilibria describing cluster formation and cavity filling.

Equilibria	Equilibrium constants[a]
$L + X \rightleftharpoons LX$	$K_1 = \frac{[LX]c^{\varnothing}}{[L][X]}$
$LX + X \rightleftharpoons LX_2$	$K_2 = \frac{[LX_2]c^{\varnothing}}{[LX][X]}$
.	.
.	.
.	.
$LX_{n-1} + X \rightleftharpoons LX_n$	$K_n = \frac{[LX_n]c^{\varnothing}}{[LX_{n-1}][X]}$

[a] The symbol $c^{\varnothing}$ stands for the concentration unit in order to make sure that the equilibrium constants are dimensionless.

$$c_i = c_0[X]^i \prod_{j=1}^{i} K_j \tag{10}$$

A simplification of eqn (10) is possible if the adsorptive-adsorbate binding strength does not or only very weakly depend on the amount of adsorptive already bound, which means that K_j is equal to the equilibrium constant K. It applies similarly for cluster formation as for cavity filling. This condition is expected to hold for the adsorptives Ar and N_2 investigated in the present study. The following arguments apply similarly if it is necessary to distinguish between two or more interactions. The result is then a corresponding linear combination of expressions addressing the individual situations, similarly to our discussion in Ref. [28]. We show this in the SI5. However, it turns out not to be needed in the present study, which means that eqn (10) can be simplified as follows:

$$c_i = c_0([X]K)^i \tag{11}$$

The total concentration of X is equal to the sum of the concentrations c_i multiplied by the number i of X bound according to the equilibria expressed in Table 1.

$$c_{tot} = \sum_{i=1}^{n} i \cdot c_i \tag{12}$$

The algebraic equality of cluster formation and of cavity filling ends here. We must now distinguish between them, and we start with the cluster formation equilibria.

3.1. Adsorption by cluster formation on a monolayer

To find the description for cluster formation we substitute c_i in eqn (12) by the expression eqn (11) and use the symbol c_{clust}. We also specify the equilibrium constant K as K_{clust}. Hence, the concentration of species that are present in the adsorbed clusters as a function of the concentration of free adsorptive X can be expressed as follows:

$$c_{clust} = c_0 \sum_{i=1}^{n} i([X]K_{clust})^i \tag{13}$$

This equation converges rapidly for situations where the product $q = [X]K_{clust}$, which has only positive values, is smaller than 1, a condition that is easily met as we shall see. We write therefore:

$$c_{clust} = c_0 \sum_{k=0}^{\infty} kq^k = c_0 \left\{ \sum_{k=0}^{\infty} (k+1)q^k - \sum_{k=0}^{\infty} q^k \right\} \tag{14}$$

This equation converges for $0 \le q < 1$ and leads to the interesting result in eqn (15).

$$c_{clust} = c_0 \frac{q}{(1-q)^2} \tag{15}$$

We insert the expression for q and write eqn (16):

$$c_{clust} = c_0 \frac{[X]K_{clust}}{(1-[X]K_{clust})^2} \tag{16}$$

In the isotherms we investigate the volume of the adsorbed gas and measured as a function of the relative pressure p_{rel} of the adsorptive X. Using the ideal gas law for expressing the concentration of X in the gas phase according to eqn (17), we write eqn (18), where p_0 is the saturation pressure of the gas at the experimental temperature, as introduced in eqn (1).

$$[X] = \frac{p_0}{RT} p_{rel} \tag{17}$$

$$[X]K_{clust} = p_{rel}\left(\frac{p_0}{RT}K_{clust}\right) \tag{18}$$

It is convenient to replace the expression in parenthesis, which is dimensionless, by the symbol k_C.

$$k_C = \left(\frac{p_0}{RT}K_{clust}\right) \tag{19}$$

The total amount of X adsorbed into clusters is measured in terms of adsorbed volume ΔV_{clust} and the parameter c_0, according to eqn (15,16), which we name V^0_{clust}. Using this we can write the final result, eqn (20), which describes the amount of adsorptive adsorbed as clusters as a function of the relative pressure.

$$\Delta V_{clust} = V^0_{clust} \frac{k_C p_{rel}}{(1-k_C p_{rel})^2} \tag{20}$$

It is convenient to write this in terms of the fractional coverage Θ_{clust} by dividing eqn (20) by the adsorbed volume for total monolayer coverage V_{mL}, as we have explained in eqn (2). We can thus express this in terms of fractional amount of cluster-bonded X as follows:

$$\Theta_{clust} = \Theta^0_{clust} \frac{k_C p_{rel}}{(1-k_C p_{rel})^2} \tag{21}$$

This is the final result which describes the cluster formation on a surface covered by one or eventually also more than one monolayer of adsorptive X. When using this equation we must pay attention to the condition that the parameter q and hence also the product $k_C p_{rel}$ must be positive and smaller than 1. Fig. 2(A) illustrates the dependence of Θ_{clust} on the relative pressure p_{rel} for different values of the constant k_C. We observe that the shape of the curve is very sensitive to the value of the equilibrium constant.

3.2. Adsorption by cavity filling

The description of cavity filling must take into account that the number of cavities is limited and therefore also the amount of adsorptive that can be bound by them. Equations (11) and (12) remain valid and in eqn (13) we need only to substitute the symbols c_{clust} and K_{clust} by c_{cav} and K_{cav}, respectively. Hence, the concentration of species adsorbed into cavities as a function of the concentration of free adsorptive X can be expressed by means of eqn (22)

$$c_{cav} = c_0 \sum_{i=1}^{n} i([X]K_{cav})^i \tag{22}$$

We denote the total concentration of cavities bearing adsorption sites for X as Λ_{cav} and express it by means of eqn (23):

$$\Lambda_{cav} = c_0 + \sum_{i=1}^{n} c_i \tag{23}$$

The relative coverage Q_{cav} of the cavities by the adsorptive X is therefore equal to the ratio of c_{cav} and Λ_{cav}:

$$Q_{cav} = \frac{c_{cav}}{\Lambda_{cav}} \tag{24}$$

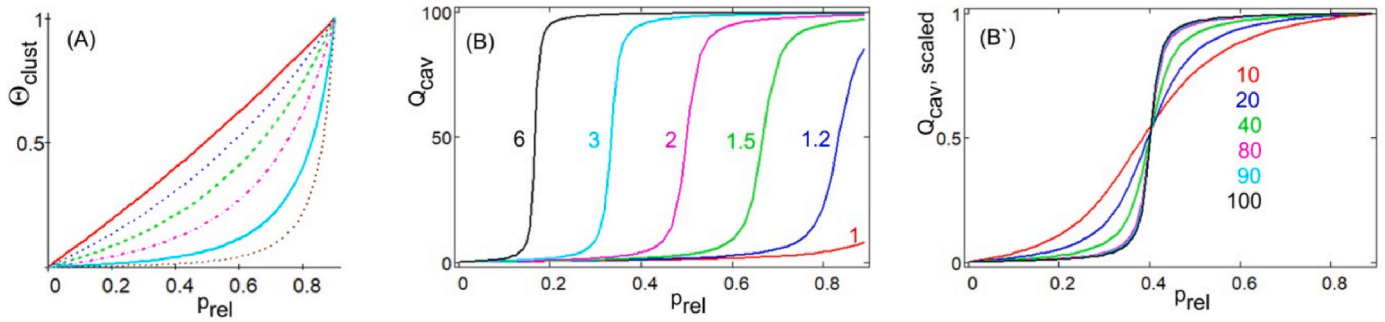

Fig. 2. Illustration of eqn (21), (A), and eqn (26), (B,B′), describing cluster formation and cavity filling, respectively. (A): Dependence of the fractional coverage Θ_{clust} by cluster-bonded X as a function of the relative pressure for different values of the constant k_C according to eqn (21). The values of Θ_{clust} are scaled to the same height at $p_{rel} = 0.9$; red solid: $k_C = 0.1$; blue dot: $k_C = 0.3$; green dash: $k_C = 0.5$; violet dash-dot: $k_C = 0.7$; light blue solid: $k_C = 0.9$; brown dot: $k_C = 1$. (B) and (B′): Dependence of the relative coverage Q_{cav} on the parameters k_{cav} and n as a function of the relative pressure p_{rel}. (B): Q_{cav} is shown for the values k_{cav} equal to 1, 1.2, 1.5, 2, 3, and 6 as indicated in the figure for equal values of n = 100. (B′) illustrates the scaled value of Q_{cav} (Q_{cav}/max(Q_{cav})) for n = 10, 20, 40, 80, 90, 100 for equal values of $k_{cav} = 2.5$. (For interpretation of the references to colour in this figure legend, the reader is referred to the Web version of this article.)

Substituting c_{cav} by means of eqn (22) and c_i by the expression (11) leads to eqn (25).

$$Q_{cav} = \frac{\sum_{i=1}^{n} i([X]K_{cav})^i}{1 + \sum_{i=1}^{n} ([X]K_{cav})^i} \tag{25}$$

There is a formal resemblance to the equilibria formulated for protein interactions with small molecules [39] and discussed recently in connection with aspects of type IV and type V isotherms [40]. The concentration [X] can be substituted by p_{rel} the same way as explained in eqn (17) - (19). This leads to eqn (26) for the relative coverage Q_{cav} as a function of the relative pressure p_{rel}.

$$Q_{cav} = \frac{\sum_{i=1}^{n} i(p_{rel}k_{cav})^i}{1 + \sum_{i=1}^{n} (p_{rel}k_{cav})^i} \; with \; k_{cav} = \left(\frac{p_0}{RT}K_{cav}\right) \tag{26}$$

We can, of course, not apply the extrapolation to very large values of n, as we have done for cluster formation, because the number of available sites in the cavities is limited [44]. It is instructive to get an idea regarding the dependence of Q_{cav} not only on the value of the equilibrium constant but also on the number n of X in a fully occupied cavity. This information is presented in Fig. 2(B,B').

We observe, that eqn (26) describes the step seen in the difference $\Delta\Theta$ we have reported in Fig. 1 for the isotherms of the mesoporous silica adsorbents. The value of p_{rel} at which this step occurs is very sensitive to the value of the equilibrium constant. The dependence of the steepness on the number of positions n in the cavity is significant for values smaller than about 80. This means that the number of n can be distinguished by means of adsorption isotherms only for very small cavities with $n < 80$. It follows that the description remains valid for situations where not all cavities are of the same size but distributed within a certain range. We will in such cases therefore always use n = 100 in our analysis. This correspond for argon to a cavity diameter of about 2 nm and means that their size is at least as large but can also be larger. The participation of the relative coverage to the fractional coverage according to eqn (26) is Θ_{cav}, which is equal to Q_{cav} multiplied by a factor abbreviated as Θ^0_{cav}. We therefore write eqn (27):

$$\Theta_{cav} = \Theta^0_{cav} Q_{cav} \tag{27}$$

Cavity filling does not explain the moderate increase of the $\Delta\Theta$ curve observed in Fig. 1(C) prior to the step. It is the signature for the formation of a second monolayer on top of the first one as expressed by eqn (6B). This is in line with results obtained by Carvalho et al. in a theoretical analysis based on advanced Monte Carlo simulations including the influence of surface irregularity and amorphous hexagonal pores. The authors observed an initially rapid increase in the adsorbate amount at very low relative pressures corresponding to the monolayer formation. As the pressure is increased, additional multilayers are gradually adsorbed, followed by a sudden step in the same range of p_{rel} corresponding to capillary condensation in uniform and regular pores [45]. The total amount of X adsorbed into cavities is measured in terms of adsorbed volume ΔV_{cav} and can be expressed analogous to eqn. (20) as follows:

$$\Delta V_{cav} = \Theta^0_{cav} V_{mL} \frac{\sum_{i=1}^{n} i(p_{rel}k_{cav})^i}{1 + \sum_{i=1}^{n} (p_{rel}k_{cav})^i} \tag{28}$$

3.3. Comparison of monolayer formation, cluster formation, and cavity filling

Equations (21) and (27) allow comparing the shape of isotherms resulting from the formation of monolayers, clusters on top of such monolayers, and cavity filling. We refer to situations, where monolayer formation is described as linear combination of Langmuir isotherms as expressed in eqn (29) [10,11,28]. We use the combination of two isotherms, because it has been observed to be adequate for many situations [12–27,29].

$$\Theta_{mL} = \frac{1}{V_{mL}} \sum_i a_i \frac{KL_i p_{rel}}{1 + KL_i p_{rel}} \tag{29}$$

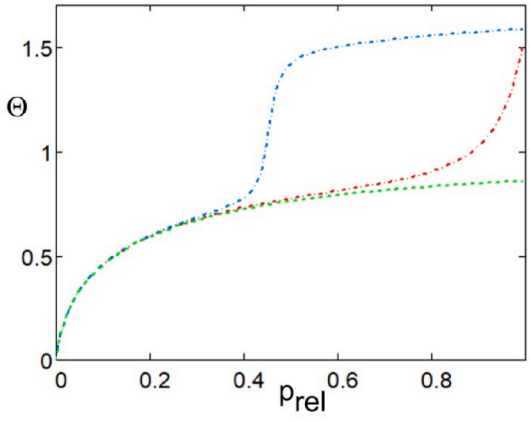

Fig. 3. Graphical representation of the adsorption isotherms. The monolayer coverage $\Theta = \Theta_{mL}$ is shown as green dash line. Cluster formation, eqns (4) and (21) $\Theta = \Theta_{mL} + \Theta_{clust}$, is shown as red dash-dot line, and the characteristic shape of cavity filling, eqns (6A) and (27) $\Theta = \Theta_{mL} + \Theta_{cav}$, is shown as blue dash-dot line. The parameters used are reported in SI3. (For interpretation of the references to colour in this figure legend, the reader is referred to the Web version of this article.)

The graphical representation of the adsorption isotherms by monolayer coverage $\Theta = \Theta_{mL}$ eqn (29) with i = 1,2, by additional cluster formation, eqn (4), $\Theta = \Theta_{mL} + \Theta_{clust}$, and by additional cavity filling, eqn (6A), $\Theta = \Theta_{mL} + \Theta_{cav}$ is presented in Fig. 3. The shape of the isotherms corresponds to type I, type II and type IV according to IUPAC classification [5,6]. Fig. 3 illustrates very nicely the characteristically different shape of the monolayer formation process, the formation of clusters, and the cavity filling on top of the monolayer.

This concludes the theoretical section and we move to the analysis of experimental data, where we evaluate to what extent this description can account for the experimental observations and whether additional information can be extracted.

4. Results and discussion

We apply the results reported in the theoretical section to the analysis of three different adsorbents, the nonporous Stöber-type silica particles, the microporous zeolite L, and the mesoporous MCM-41 as reported in Fig. 1 and Figs. SI1-SI4. The examination of the experimental data includes the previously communicated low relative pressure investigation using lc2-L (linear combination of 2 Langmuir isotherms) [29], where the specific surface area, the volume of adsorptive bound as a monolayer, and the binding strength are reported.

4.1. Adsorption by cluster formation on a monolayer

We start with the analysis of adsorption isotherms of the nonporous Stöber-type particles. These silica particles are well-known for their almost perfect spherical morphology, their low polydispersity, and as excellent nonporous reference materials for the investigation of adsorption processes, provided that they have been calcined to remove any residual microporosity [30,46]. The surface area of the samples used in the present study amounts to 14 m^2/g. Two sites were identified at which the monolayer is formed, with the adsorption enthalpies $\Delta_{ads}H_1^{\varnothing} = -11$ kJ/mol and $\Delta_{ads}H_2^{\varnothing} = -8$ kJ/mol. The relative contribution of the two sites is approximately 0.8:3, Table 2 of ref. [29]. No indication of a second monolayer formation is observed. Instead, cluster formation on top of the first monolayer takes place as illustrated in Fig. 1(A). This cluster formation equilibrium can be analyzed using eqn (21). The result is reported in Fig. 4 for Ar isotherms measured at 87 K and at 77 K and for an isotherm using N_2 as adsorptive and measured at 77 K. A comparison of the calculated Θ_{clust} and the difference $\Delta\Theta$ between the experimental adsorption isotherm Θ_{exp} and the monolayer coverage, eqn (3), as a function of the relative pressure p_{rel} is presented. The calculated Θ_{clust} values plotted as red lines compare well with the difference $\Delta\Theta$ marked as blue line. This is supported by the residuals, which is the difference between $\Delta\Theta$ and Θ_{clust}, shown as green dash-dot curves.

The constants resulting from this analysis are collected in Table 2. The values of free enthalpy $\Delta_{clust}G$ and also of the binding enthalpy $\Delta_{clust}H$ of cluster formation, as determined using eqn (34) in Ref. [29], are smaller than those of the monolayer formation, as expected. They are, however, larger than the enthalpy of vaporization which amounts to 6.506 kJ/mol for Ar and to 5.586 kJ/mol for N_2 at the respective transition temperatures [47]. The inflection point marks the point where the curvature of the adsorption isotherm changes sign. It can be calculated by evaluating the second derivative of Θ, which vanishes at this point according to eqn (30).

$$\frac{d^2}{dp_{rel}^2}\Theta = 0 \tag{30}$$

The algebra of the calculation is outlined in the SI, section SI2. We observe in Table 2 that the calculated inflection points and the experimental values match. It is interesting to compare the volume adsorbed by monolayer formation V_{mL} and the volume adsorbed by cluster formation ΔV_{clust} at $p_{rel} = 0.9$. This can be calculated using eqn (31), derived from eqn (20).

$$\Delta V_{clust}^{0.9} = \Theta_{clust}^{0} V_{mL} \frac{0.9k_C}{(1-0.9k_C)^2} \tag{31}$$

We observe that the amount of adsorptive bound by cluster formation at $p_{rel} = 0.9$, 87 K, is roughly 1.4 times larger than that adsorbed as a monolayer. We would also like to know how the calculated fractional coverage Θ_{calc} according to eqn (4) compares with the experimental values Θ_{exp} over the whole range $0 < p_{rel} \leq 0.9$. The comparison

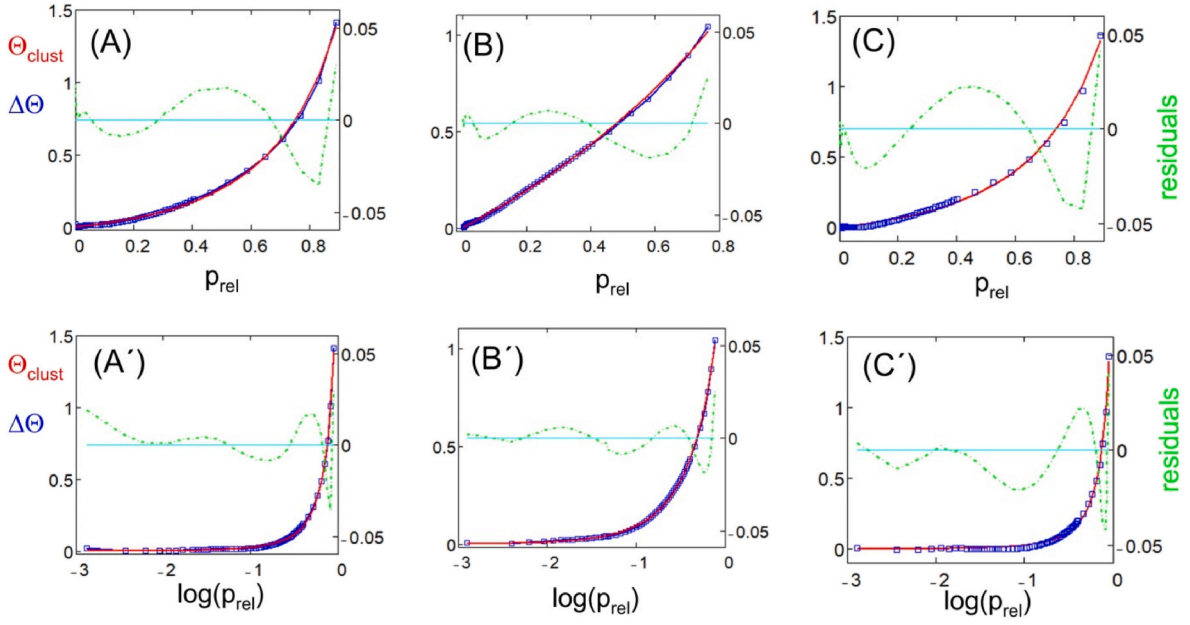

Fig. 4. Analysis of cluster formation on Stöber-type adsorbents. Blue squares: Difference ΔΘ between Θ_{exp} and the lc2-L Langmuir isotherm, eqn (3). Red solid: Calculated isotherm Θ_{clust} according to eqn (21). Green dash-dot: Residuals (difference between ΔΘ and Θ_{clust}), right axis. Light blue line: Zero reference for residuals. (A,A') Ar at 87 K, (B,B') Ar at 77 K, and (C,C') N_2 at 77 K. (For interpretation of the references to colour in this figure legend, the reader is referred to the Web version of this article.)

Table 2
Results for the Stöber-type silica particles.

Adsorptive	V_{mL}[a] [cm^3/g]	$\Delta V^{0.9}_{clust}$ [cm^3/g]	K_{clust} (k_C)	Θ^0_{clust}	$\Delta_{clust}H_i^{\varnothing}$ [kJ/mol]	$\Delta_{clust}G_i^{\varnothing}$ [kJ/mol]	infl. point[a] exp [p_{rel}]	infl. point calc [p_{rel}]
Ar p_0 = 1.069 bar, 87 K	3.7	5.3	4.73 (0.70)	0.31	−7.56	−1.08	0.35	0.34
Ar p_0 = 0.260 bar, 77 K	2.8	–	23.3 (0.25)	3.6	−7.76	−2.02	0.35	0.36
N_2 p_0 = 0.983 bar, 77 K	3.3	4.6	4.41 (0.67)	0.38	−6.69	−0.95	0.26	0.29

[a] From ref [29].

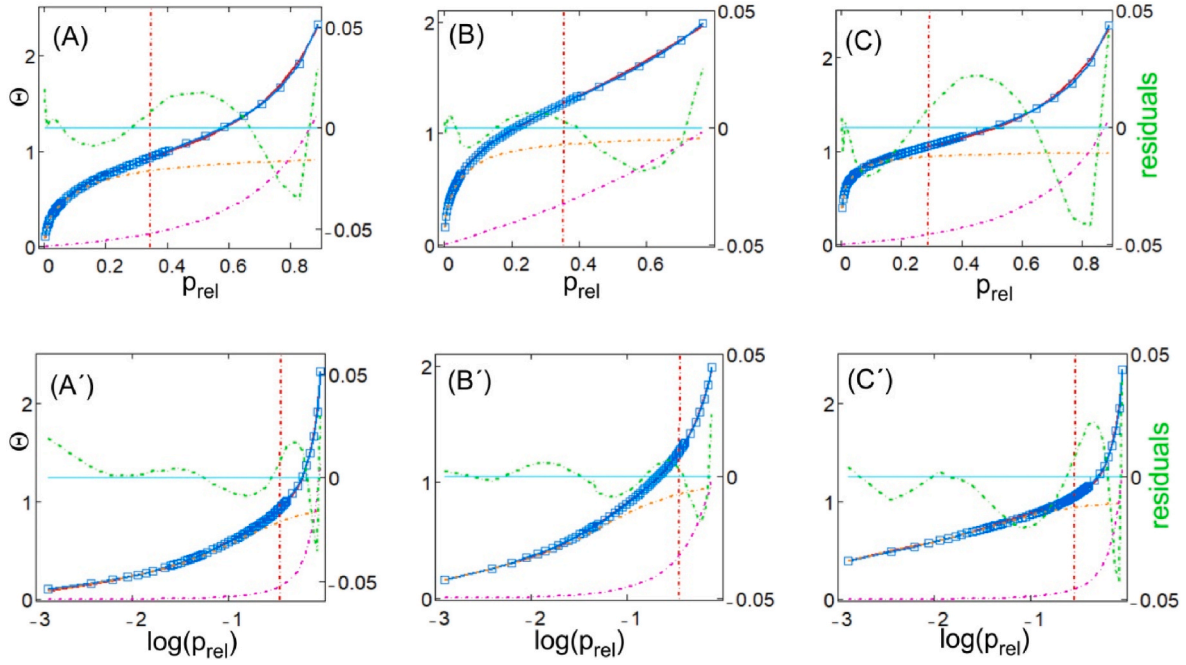

Fig. 5. Stöber-type particles, complete isotherms. (A,A') Ar at 87 K; (B,B') Ar at 77 K; (C,C') N_2 at 77 K. Blue squares: Experimental isotherms Θ_{exp} versus the relative pressure p_{rel} and versus log(p_{rel}). Red solid: Calculated isotherm Θ_{calc} according to eqns (4) and (21). Green dash-dot: Residuals (difference Θ_{exp} - Θ_{calc}), right axis. Light blue line: Zero reference for residuals. The position of the calculated inflection point is shown as red vertical dash-dot line. It matches with the experimental one. The contributions of the monolayer adsorption Θ_{mL} and the cluster formation Θ_{clust} are shown as an orange and as a violet dash-dot line, respectively. (For interpretation of the references to colour in this figure legend, the reader is referred to the Web version of this article.)

reported in Fig. 5 shows good agreement. This supports our theoretical reasoning.

4.2. Formation of a second monolayer and adsorption by cluster formation

We have observed that extensive monolayer coverage is already realized at small relative pressure for the microporous zeolite L and that the S-shape of the ΔΘ curve in Fig. 1(B) indicates the presence of two processes. The monolayer is more strongly bound to the highly polar surface of zeolite L than for the Stöber-type particles. The consequence is that large coverage is already realized at low relative pressure, which favors the formation of a second monolayer, expressed as Θ_{2L}, on top of the first one, before cluster formation, which minimizes surface tension, starts. This means that eqn (4) must be extended as expressed in eqn (5). The formation of a second monolayer on top of the first one is expressed in eqn (32), where a_{2L} measures the amount of adsorptive bound as a second monolayer and K'_{2L} is the corresponding equilibrium constant.

$$\Theta_{2L} = a_{2L}\frac{K'_{2L}p_{rel}}{1 + K'_{2L}p_{rel}} \tag{32}$$

The result of this description is reported in Fig. 6 and in Table 3 for zeolite L (A), and for Indigo-ZL (B). The agreement between experimental data Θ_{exp} and the calculated values Θ_{calc}, seen in Fig. 6 (A,A') and (B,B'), is good. The contribution of the monolayer coverage Θ_{mL} is indicated as orange dash-dot line. The residuals $\Theta_{exp} - \Theta_{calc}$ are well distributed. It is interesting to compare the contributions of the second monolayer Θ_{2L} formed on top of the first one and the contribution due to cluster formation Θ_{clust}. This comparison is shown in Fig. 6 (A″) and (B″) where we see the difference ΔΘ between the experimental adsorption isotherm Θ_{exp} and the lc2-L monolayer coverage isotherm Θ_{mL} according to eqn (2). The red solid lines show the calculated isotherm $\Delta\Theta_{calc} = \Theta_{2L} + \Theta_{clust}$. The dark-green and pink dash-dot lines illustrate the individual contributions Θ_{clust} and Θ_{2L}, respectively. We observe for zeolite L, Fig. 6(A″), that the second monolayer has been developed to a large extent before cluster formation takes place. This means that clusters are formed on top of the second monolayer. Both contributions to ΔΘ are about the same at $p_{rel} = 0.9$. The volume adsorbed by cluster formation $\Delta V^{0.9}_{clust}$ calculated using eqn (22) amounts to 12 cm^3/g and is therefore less significant than the monolayer coverage volume V_{mL}, which is 88 cm^3/g, see Table 3. The cluster binding enthalpy $\Delta_{clust}H_i^{\varnothing}$ is slightly less favorable with respect to that for the second monolayer $\Delta_{ads}H^{\varnothing}_{2L}$. However, both are favorable with respect to the enthalpy of vaporization, which amounts to 6.506 kJ/mol, as we have mentioned above. The situation is less pronounced for Indigo-ZL, where we observe, in contrast, that the relative contribution of the volume $\Delta V^{0.9}_{clust}$ for cluster formation at $p_{rel} = 0.9$ is more important than the monolayer coverage volume and that it exceeds the value due to the second monolayer formation. The monolayer coverage volume V_{mL} of the Indigo-ZL adsorbent is, however, small with respect to the pristine zeolite L, because the

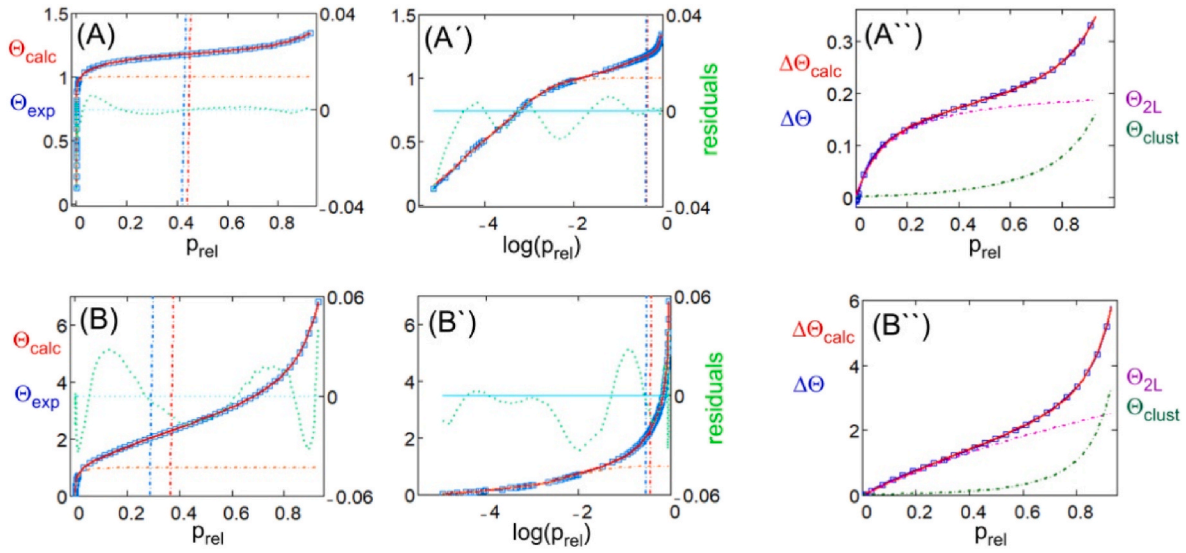

Fig. 6. Analysis of ZL (top), and of Indigo-ZL (bottom) isotherms. Ar at 87 K. (A,A′) and (B,B′): The blue line marked by squares denotes the experimental isotherms Θ_{exp}. The red solid line shows the calculated isotherms Θ_{calc} according to eqn (5) and the orange dash-dot curve shows the contribution of Θ_{mL}. Green dash-dot lines are the residuals. Light blue line: Zero reference for residuals. The positions of the experimental and the calculated inflection points are shown by blue and red vertical dash-dot lines. (A″,B″) show the $\Delta\Theta$ between the experimental adsorption isotherm Θ_{ads} and the lc2-L monolayer coverage isotherm Θ_{mL}. The red solid lines show the calculated isotherm $\Delta\Theta_{calc} = \Theta_{2L} + \Theta_{clust}$ and the green and pink dash-dot lines illustrate the individual contributions Θ_{clust} and Θ_{2L}, respectively. (For interpretation of the references to colour in this figure legend, the reader is referred to the Web version of this article.)

Table 3
Results for ZL and Indigo-ZL adsorbents. (Adsorptive: Ar, $p_0 = 1.069$ bar, 87 K).

Adsorbent	V_{mL}[a] [cm^3/g]	$\Delta V^{0.9}_{clust}$ [cm^3/g]	K_{clust}/k_C	Θ^0_{clust}	$\Delta_{clust}H^{\varnothing}$ [kJ/mol]	$\Delta_{clust}G^{\varnothing}$ [kJ/mol]	K_{2L}/a_{2L}	$\Delta_{ads}H^{\varnothing}_{2L}$ [kJ/mol]	$\Delta_{ads}G^{\varnothing}_{2L}$ [kJ/mol]	infl. point exp[a]/calc [p_{rel}]
ZL	88	12	4.81/0.76	1.74	−7.6	−1.14	7.67/18.5	−7.9	−1.4	0.42/0.45
Indigo-ZL	3.5	9	5.58/0.88	0.48	−7.7	−1.24	0.45/29.4	−5.9	0.58	0.30/0.37

[a] From ref [29].

pores are blocked by the indigo molecules. As a consequence, only the outer surface of the particles is accessible, so that this sample resembles a nonporous adsorbent. The cluster binding enthalpies $\Delta_{clust}H^{\varnothing}_i$ for the Stöber-type silica and for ZL at 87 K are equal, and that of the Indigo-ZL differs by a non-significant amount. We observe that the calculated and the experimental inflection points differ very little for zeolite L. They also agree well for Indigo-ZL.

The value $\Delta V^{0.9}_{clust}$ is small with respect to V_{mL} for ZL but larger for

Table 4
Results for the mesoporous silica adsorbents with Ar and N_2 as adsorptive. (Ar, $p_0 = 1.069$ bar, 87 K; N_2, $p_0 = 0.983$ bar, 77 K).

Adsorbent Adsorptive	V_{mL}[a] [cm^3/g]	$\Delta V^{0.9}_{cav}$ [cm^3/g]	K_{cav}/k_C	Θ^0_{cav}	$\Delta_{cav}H^{\varnothing}$ [kJ/mol]	$\Delta_{cav}G^{\varnothing}$ [kJ/mol]	K_{2L}/a_{2L}	$\Delta_{ads}H^{\varnothing}_{2L}$ [kJ/mol]	$\Delta_{ads}G^{\varnothing}_{2L}$ [kJ/mol]	infl. pt. exp[a]/calc [p_{rel}]	Second infl. pt. calc [p_{rel}]
MCM-41 (4.4 nm) Ar, 87 K	251	342	14.3/2.3	0.014	−8.4	−1.9	0.42/437	−5.8	0.64	0.24/0.28	0.44
MCM-41 (4.1 nm) Ar, 87 K	286	311	16.5/2.6	0.011	−8.5	−2.0	0.86/174	−6.4	0.11	0.24/0.25	0.38
MCM-41 (2.7 nm) Ar, 87 K	208	46	37.3/5.9	0.007	−9.1	−2.6	[b])	[b])	[b])	0.09/0.11	0.17
MCM-41 (4.4 nm) N_2, 77 K	151	168	16.3/2.5	0.011	−7.5	−1.8	0.93/333	−5.7	0.05	0.22/0.25	0.41
MCM-41 (4.1 nm) N_2, 77 K	169	170	19.6/3.0	0.010	−7.6	−1.9	2.3/189	−6.3	−0.54	0.21/0.22	0.34
MCM-41 (2.7 nm) N_2, 77 K	100	36	54/8.1	0.012	−8.3	−2.6	3.4/40	−6.5	−0.78	0.07/0.07	0.12

[a] From ref [29].
[b] These parameters could not be determined reliably and are therefore omitted.

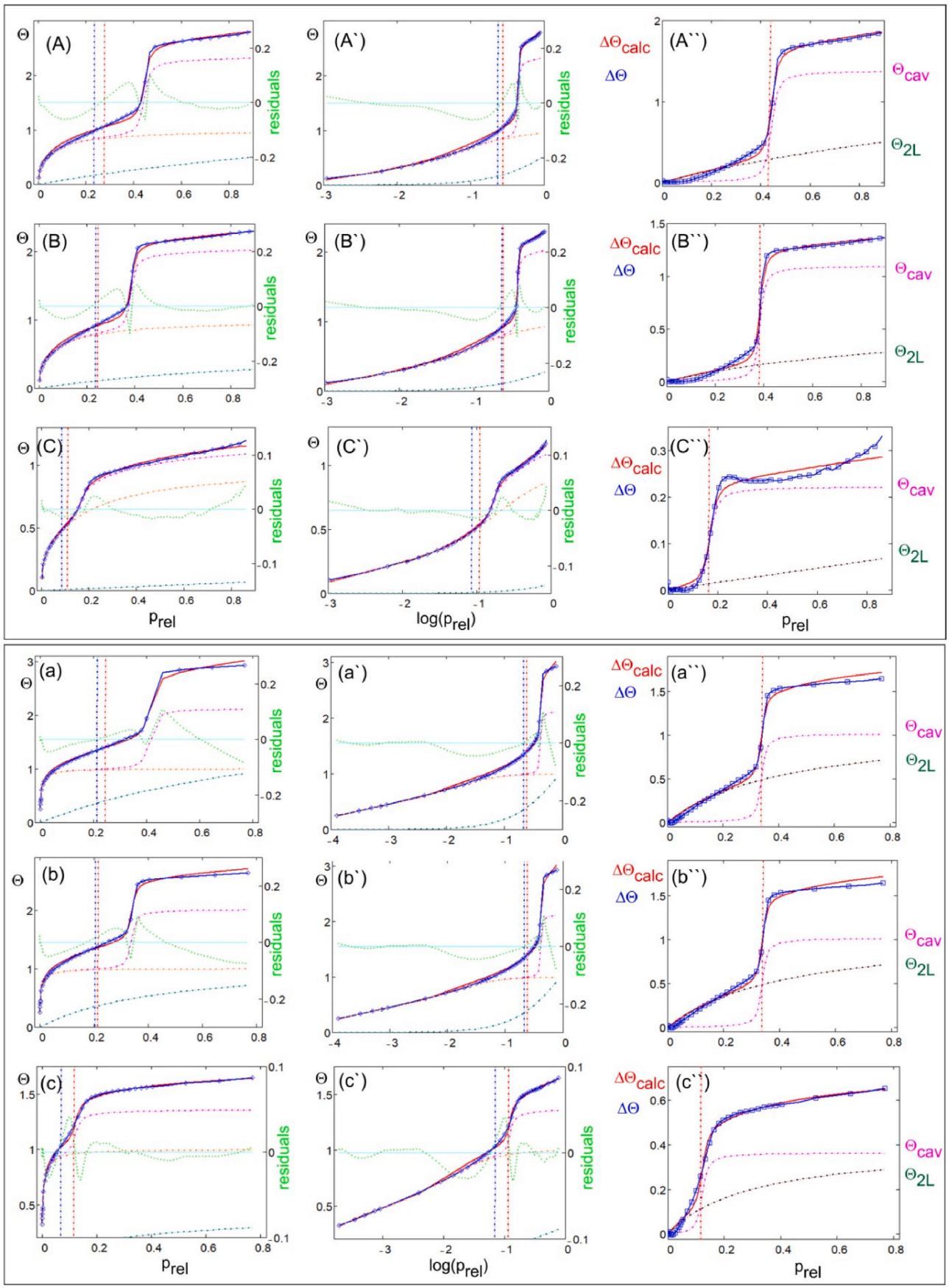

(caption on next page)

Fig. 7. Isotherms of mesoporous silica MCM-41. (A,B,C): Ar at 87 K. (a,b,c): N_2 at 77 K. (A),(a) MCM-41 (4.4 nm); (B),(b) MCM-41 (4.1 nm); (C),(c) MCM-41 (2.7 nm). Blue lines marked by squares: Experimental isotherms Θ_{exp}. Red solid lines: Calculated isotherms Θ_{calc}. Green dotted lines: Residuals. Light blue line: Zero reference for the residuals. Blue and red vertical dash-dot lines: Experimental and the calculated position of the inflection point in (A,B,C) and (a,b,c). The orange, the dark green, and the pink dash-dot curves show the contributions of Θ_{mL}, of Θ_{2L}, and of Θ_{cav} to Θ. The blue lines marked by squares seen in (A″,B″,C″) and (a”,b”,c”) show the difference $\Delta\Theta$ between the experimental isotherm Θ_{exp} and the lc2-L monolayer coverage isotherm Θ_{mL}. The red solid lines show the calculated isotherm $\Delta\Theta_{calc} = \Theta_{2L} + \Theta_{cav}$ and the pink and the green dash-dot lines are the individual contributions Θ_{cav} and Θ_{2L}, respectively. Red vertical dash-dot lines: Position of the calculated second inflection point. (For interpretation of the references to colour in this figure legend, the reader is referred to the Web version of this article.)

Indigo-ZLIt is, however, similar for both adsorbents and indicates that cluster formation takes place exclusively at the outer surface, which is of similar magnitude for both adsorbents. This is supported by the fact that the $\Delta_{clust}H^{\varnothing}$ values are practically the same.

4.3. Formation of a second monolayer and adsorption by cavity filling

We have seen in Fig. 1(C), SI3, and SI4 that the $\Delta\Theta$ curve shows, after an initial period, first a moderate increase followed by a step and a nearly flat continuation for all mesoporous silica adsorbents for both adsorptives Ar and N_2. The adsorption isotherms resemble in all cases the blue dash-dot curve in Fig. 3 which describes the $\Theta = \Theta_{mL} + \Theta_{cav}$ function. They also show, however, an additional contribution which can be attributed to a second monolayer formation Θ_{2L}. This means that eqn (6B) is adequate for describing the mesoporous silica adsorption isotherms. The result of this description is reported in Table 4 and in Fig. 7, where we compare the calculated isotherms with the experimental ones and where we also add the individual contributions Θ_{mL}, Θ_{2L}, and Θ_{cav}. The agreement between calculated and experimental values is convincing and supported by the residuals. It is remarkable how well the calculated and the experimental inflection points match. This applies also for the calculated second inflection point, which is characteristic for this type of isotherms. We observe that the values for the cavity filling enthalpy $\Delta_{cav}H^{\varnothing}$ are slightly larger than those found for the cluster formation in Tables 2 and 3. They are significantly smaller than those measured for monolayer formation as reported in Tables 2 and 4 of ref [29]. The values for the second monolayer formation $\Delta_{ads}H^{\varnothing}_{2L}$, however, underline what is seen in Fig. 7, namely that this process plays a less important role, which nevertheless influences the shape of the isotherms, so that it cannot be neglected. The second monolayer formation for the Ar isotherm of MCM-41 (2.7 nm) is, however, so weak, that the thermodynamic parameters could not be determined reliably and are therefore omitted in Table 4. It is interesting to observe that the volume adsorbed by cavity filling ΔV_{cav} at $p_{rel} = 0.9$ as described in eqn (32), which can be derived analogous to eqn (31), is larger or at least equal to V_{mL} for pore diameters of 4.4 nm and 4.1 nm, but significantly smaller than V_{mL} for mesoporous silica with a pore diameter of 2.7 nm. This applies for both Ar and N_2 as adsorptive.

$$\Delta V^{0.9}_{cav} = \Theta^{0}_{cav} V_{mL} \frac{\sum_{i=1}^{n} i(0.9k_{cav})^{i}}{1 + \sum_{i=1}^{n}(0.9k_{cav})^{i}} \tag{33}$$

5. Conclusions

The adsorption of simple gases begins with the formation of a monolayer on the pristine surface, sometimes followed by the formation of a second or more monolayers. Subsequently, cluster formation on top of the layer or cavity filling occurs, depending on the properties of the surface. This means that the adsorption isotherms must be understood as the signature of several sequential chemical equilibrium steps [48]. The characteristically different shape of the isotherms related to these processes allows differentiation. However, it is custom to analyze only specific pressure ranges of the isotherms quantitatively, usually the region which allows determining the specific surface area, the volume of adsorptive bound as a monolayer, and the enthalpy of adsorption. Hence, only part of the information provided by the adsorption isotherms is extracted. Our aim is to analyze the isotherms quantitatively over the entire relative pressure range. Ar and N_2 adsorption isotherms were investigated for adsorbents bearing different properties: the nonporous Stöber-type particles, the microporous zeolite L, zeolite L filled with indigo, and three mesoporous silica adsorbents with different pore sizes. We analyzed the equilibria which resulted in cluster formation and those which resulted in cavity filling. The formal equilibria can be expressed for both cases in the same way. They differ in terms of the conditions, which means no restriction for cluster growth and limitation by the extension of cavities which limits the space for accepting adsorptive. The equations describing the relative coverage due to cluster formation and the relative coverage due to cavity filling have been derived, eqn (21) and eqn (26), respectively. They have been successfully used, by applying the results for monolayer formation reported previously [29], to quantitatively describe the complete isotherms of nonporous, microporous and mesoporous adsorbents. It is interesting that no indication for the formation of a second monolayer on top of the first one is observed for the Stöber-type particles. Instead, cluster formation, which minimizes surface tension, starts early. The behavior of the microporous zeolite L and the Indigo-ZL is substantially different. A second monolayer emerges and cluster formation starts with some delay. The enthalpy of cluster formation is, however, practically identical with that seen for the Stöber-type particles. A finding which makes sense, because the clusters formed have the same purpose, namely to minimize surface tension. In addition, the difference between the experimental and the calculated inflection points is very small, a fact which underlines the correctness of the description. The shape of the isotherms for the mesoporous silica adsorbents differs very much from those seen for the nonporous and for the microporous adsorbents as illustrated in Fig. 1(C), where we have discussed that the $\Delta\Theta$ curve shows, after an initial period, first a moderate increase followed by a sharp step and a near flat continuation. The quantitative analysis of the data proves that formation of a second monolayer is followed by filling of cavities which ends as soon as all cavity sites are filled. This is illustrated in Fig. 7 for Ar isotherms measured at 87 K and for N_2 isotherms measured at 77 K. In this Figure the individual contributions are shown, namely the monolayer formation Θ_{mL}, the appearance of a second monolayer expressed as Θ_{2L}, and the fractional cavity filling contribution Θ_{cav}. The sum of these contributions constitutes the calculated adsorption isotherm Θ_{calc}, which compares well with the experimental data Θ_{exp}. The experimental and the calculated first inflection points agree very well. This applies also for the second inflection point. The cavity filling enthalpy reported in Table 4 is roughly 10% larger than that for the cluster formation of the nonporous and the microporous adsorbents shown in Tables 2 and 3. The volume for cavity filling is significantly smaller than V_{mL} for mesoporous silica with a pore diameter of 2.7 nm, while it is the same or larger for the two other mesoporous silica adsorbents featuring pore sizes of 4.1 and 4.4 nm. We conclude that understanding the adsorption isotherms as signature of several sequential chemical equilibrium steps as reported in Ref. [29] and in the present study is not only adequate but provides us with interesting otherwise hidden additional information, such as data for clusters, cavities, and precise positions of the inflection points presented in Tables 2–4, not accessible by means of the conventional models. The theory presented covers type I, II and IV isotherms and can be extended to type VI as shown in Fig. SI5. It is based on a thermodynamic concept and applies for many situations.

Declaration of competing interest

The authors declare that they have no known competing financial interests or personal relationships that could have appeared to influence the work reported in this paper.

Acknowledgements

This work was supported by the Swiss National Science Foundation (project 200021_172805).

Appendix A. Supplementary data

Supplementary data to this article can be found online at https://doi.org/10.1016/j.micromeso.2021.111563.

Supplementary data

Supplementary data to this article has been added.

References

[1] R.M. Barrer, Zeolites and Clay Minerals as Sorbents and Molecular Sieves (Chapter 4), Academic Press, London, 1978, ISBN 0120793504.
[2] W. Rudzinski, D.H. Everett, Adsorption of Gases on Heterogeneous Surfaces, Academic Press, London, 1992, ISBN 0-12-601690-9.
[3] F. Rouquerol, J. Rouquerol, K. Sing, Adsorption by Powders and Porous Solids, Academic Press, London, 1999.
[4] M.P.L. Llewellyn, G. Maurin, in: J. Cejka, H. Bekkum, A. Corma, F. Schüth (Eds.), Introduction to Zeolite Science and Practice, third ed., Elsevier Amsterdam, 2007, pp. 556–610 (Chapter 17).
[5] T. Horikawa, D.D. Do, D. Nicholson, Adv. Colloid Interface Sci. 169 (2011) 40–58.
[6] M. Thommes, K. Kaneko, A.V. Neimark, J.P. Olivier, F. Rodriguez-Reinoso, J. Rouquerol, K.S.W. Sing, IUPAC technical report), Pure Appl. Chem. 87 (9–10) (2015) 1051–1069.
[7] T.C. Brown, D.J. Miron, Ch M. Fellows, Phys. Chem. Chem. Phys. 21 (2019) 2558–2566.
[8] N. Narayanaswamy, C.A. Ward, J. Phys. Chem. C 123 (2019) 18336–18346.
[9] a) A. Sarkar, B. Paul, Microporous Mesoporous Mater. 302 (2020) 110191; b) L. Wu, J. Liu, H. Shang, S. Li, J. Yang, L. Li, J. Li, Microporous Mesoporous Mater. 316 (2021) 110956.
[10] I. Langmuir, J. Am. Chem. Soc. 40 (1918) 1361–1403.
[11] H. Swenson, N.P. Stadie, Langmuir 35 (2019) 5409–5426.
[12] A.L. Myers, AlChE J 29 (4) (1983) 691–693.
[13] R.G. Jordi, D.D. Do, J. Chem. Soc. Faraday. Trans. 88 (16) (1992) 2411–2419.
[14] P. M. Mathias, R. Kumar, J. D. Moyer, Jr, J. M. Schork, S. R. Srinivasan, S. R. Auvil, O. Talu, Ind. Eng. Chem. Res. 351 (996) 2477-2483.
[15] A. Micke, M. Billow, M. Kocirik, P. Struve, J. Phys. Chem. 98 (1994) 12337–12344.
[16] W. Zhu, F. Kapteijn, J.A. Moulijn, Chem. Commun. (1999) 2453–2454.
[17] L. Song, L.V.C. Rees, J. Chem. Soc. Faraday. Trans. 93 (4) (1997) 649–657.
[18] T.J.H. Vlugt, R. Krishna, B. Smit, J. Phys. Chem. B 103 (1999) 1102–1118.
[19] R. Krishna, T.J.H. Vlugt, B. Smit, Chem. Eng. Sci. 54 (1999) 1751–1757.
[20] D. Paschek, R. Krishna, Phys. Chem. Chem. Phys. 2 (2000) 2389–2394.
[21] W. Zhu, F. Kapteijn, J.A. Moulijn, M.C. den Exter, J.C. Jansen, Langmuir 16 (2000) 3322–3329.
[22] J.A. Ritter, S.J. Bhadra, A.D. Ebner, Langmuir 27 (2011) 4700–4712.
[23] S. Keskin, J. Liu, J.K. Johnson, D.S. Sholl, Langmuir 24 (2008) 8254–8261.
[24] S. García, J.J. Pis, F. Rubiera, C. Pevida, Langmuir 29 (2013) 6042–6052.
[25] S.J. Bhadra, A.D. Ebner, J.A. Ritter, Langmuir 28 (2012) 6935–6941.
[26] K. Liu, B. Li, Y. Li, X. Li, F. Yang, G. Zeng, Y. Peng, Z. Zhang, G. Li, Z. Shi, S. Feng, D. Song, Chem. Commun. 50 (2014) 5031–5033.
[27] A. Farzaneh, M. Zhou, E. Potapova, Z. Bacsik, L. Ohlin, A. Holmgren, J. Hedlund, M. Grahn, Langmuir 31 (2015) 4887–4894.
[28] a) G. Calzaferri, Phys. Chem. Chem. Phys. 20 (2018) 29070–29084; b) G. Calzaferri, Phys. Chem. Chem. Phys. 19 (2017) 10611–10621.
[29] G. Calzaferri, S.H. Gallagher, D. Brühwiler, Microporous Mesoporous Mater. 312 (2021) 110744.
[30] W. Stöber, A. Fink, E. Bohn, J. Colloid Interface Sci. 26 (1968) 62–69.
[31] a) Ch Baerlocher, W.M. Meier, D.H. Olson, in: Atlas of Zeolite Framework Types, fifth ed., Elsevier, Amsterdam, 2001; (b) International zeolite association. http://www.iza-structure.org/databases.
[32] G. Calzaferri, Structure and Bonding, Springer, Berlin, 2020. https://doi.org/10.1007/430_2020_57.
[33] D. Brühwiler, H. Frei, J. Phys. Chem. B 107 (2003) 8547–8556.
[34] J.A.S. Costa, R.A. de Jesus, D.O. Santos, J.F. Mano, L.P.C. Romäod, C.M. Paranhos, Microporous Mesoporous Mater. 291 (2020) 109698.
[35] Cavity filling is often referred to as capillary condensation, however, we prefer using the more specific term “cavity filling” within the present context.
[36] P. Woodtli, S. Giger, P. Müller, L. Sägesser, N. Zucchetto, M.J. Reber, A. Ecker, D. Brühwiler, Dyes Pigments 149 (2018) 456–461.
[37] D.W. Marquardt, J. Soc. Ind. Appl. Math. 11 (1963) 431–441.
[38] The Levenberg-Marquardt Method Implemented in Mathcad 14, Mathsoft Eng. & Edu., Inc. (http://www.mathsoft.com).
[39] I.M. Klotz, Acc. Chem. Res. 7 (1974) 162–168.
[40] a) C. Buttersack, Phys. Chem. Chem. Phys. 21 (2019) 5614–5626; b) C. Buttersack, Microporous Mesoporous Mater. 316 (2021) 110909.
[41] I. Prigogine, in: Thermodynamics of Irreversible Processes, third ed., Wiley & Sons, Hoboken, NJ, USA, 1967.
[42] Th Dubler, C. Maissen, G. Calzaferri, Z. Naturforsch. 31b (1976) 569–579.
[43] G. Calzaferri, Sciforum Electronic Conf. Ser., ECEA 2017. Proceedings, 2, 2018, pp. 1–9, https://doi.org/10.3390/ecea-4-05019, 168.
[44] It is trivial that eqn (26) reduces formally to Langmuir’s equation for n=1. This should, however, not be understood as a derivation of the Langmuir isotherm equation; see ref [28].
[45] A.J.P. Carvalho, T. Ferreira, A.J.E. Candeiasa, J.P.P. Ramalho, THEOCHEM 729 (2005) 65–69.
[46] S. Li, Q. Wan, Z. Qin, Y. Fu, Y. Gu, Langmuir 31 (2015) 824–832.
[47] P.W. Atkins, J. de Paula, Physikalische Chemie, 4, Wiley-VCH Weinheim, Auflage, 2006, ISBN 3-527-31546-2.
[48] Chemical equilibrium language is Thermodynamic and therefore independent of the kind of interaction, whether this Is called physisorption or chemisorption.